were placed in a LAB-TEK glass 2-well (1×10^3 cells/well) chamber slide (Nunc, Rochester, NY, USA) together with 1 ml of the appropriate medium (MEM for U-87 MG, ACBRI 371, SK-N-SH; DMEM for OL) and incubated at 37°C, 5% CO_2 for six days. After fixation with ice-cold ethanol/acetone, cells were blocked in PBS containing 1% BSA (Sigma-Aldrich) and 10% normal horse serum (Dako) for 30 min at room temperature. After an overnight incubation at 4°C with primary antibodies, the cells were rinsed in PBS and then incubated at room temperature in the dark with secondary antibody. The primary antibodies used were as follows: polyclonal goat anti-FEZ1 antibody (1:5000; Abcam), polyclonal rabbit anti-GFAP antibody (1:200; Abcam) and monoclonal anti-NeuN antibody (1:200; Abcam). The corresponding secondary antibodies were as follows: Alexa Fluor 488 anti-goat IgG or Alex Fluor 594 anti-rabbit IgG (1:300; Invitrogen). Following incubation with the secondary antibody, the tissues were rinsed in PBS and subjected to nuclear staining with 4, 6-diamidino-2-phenylindole (DAPI) (Invitrogen). Microscopic images were captured using a Leica DAS Mikroskop microscope (Leica Microsystems, Wetzlar, Germany). To evaluate the effects of the four mood stabilizers on FEZ1 localization in U-87 MG cells, cells were cultured for five days with six different treatments (i.e., 1.2 mM Li, 1 mM VPA, 100 μM CBZ, 50 μM LTG, DMSO, and non-treated) in LAB-TEK chamber slides, and subjected to the above-mentioned immunostaining procedure.

Results

Microarray gene expression profiles

Among the 11,214 genes expressed in at least one of the 12 U-87 MG samples treated with or without mood stabilizers (6 types of media × 2 replicates = 12 samples), 65, 797, 315, and 641 genes were found to be induced with a fold change of > 1.2 (20% increase) by the Li, VPA, CBZ, and LTG treatments, respectively. In contrast, 142, 1008, 80, and 543 genes were suppressed with a fold change of < 0.833 (20% decrease) by the mood stabilizer treatments, respectively (Fig. 1). Tables 1 and 2 show gene symbols for the 10 most robustly up- and down-regulated genes in response to each mood stabilizer treatment, some of which have functions relevant to the mechanism of action of each mood stabilizer. VPA and LTG tended to affect more genes at the transcriptional level in astrocyte-derived cells, whereas the cellular effects

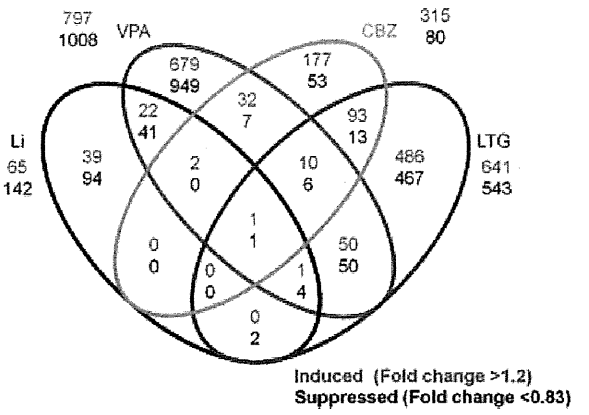

Fig. 1. Venn diagram summarizing the number of genes altered by each mood stabilizer and the overlaps among the genes altered by each mood stabilizer. Genes were selected according to the following criteria: a fold change > 1.2 (red) or < 0.83 (black) in both of the duplicated pairs of microarrays, a signal intensity > 20, and a detection p-value < 0.05 in all microarrays. Li = lithium; VPA = valproic acid; CBZ = carbamazepine; LTG = lamotrigine.

of the Li and CBZ treatments at the therapeutic concentrations used were relatively modest. Li and VPA commonly induced 26 genes and suppressed 46 genes, whereas Li demonstrated little overlap with the other anticonvulsants (3 induced genes and 1 suppressed gene in common between Li- and CBZ-treated samples; 2 induced and 7 suppressed genes in common between Li- and LTG-treated samples). The observed number of commonly regulated genes between Li- and VPA-treated samples was significantly higher than the expected number ($p < 0.001$). Furthermore, the observed number of commonly induced/suppressed genes between CBZ- and LTG-treated samples (104 and 20 genes, respectively) was also significantly higher than the expected number ($p < 0.001$). Hierarchical clustering analysis of the signal intensity ratio of mood-stabilizer-treated cells divided the four mood stabilizers into two groups, Li-VPA and CBZ-LTG (Fig. 2), which was consistent with the numbers of overlapping genes among the four mood stabilizers.

Induction of FEZ1 expression in human astrocytic cells

FEZ1 was the only gene induced by all four mood stabilizers. The microarray data revealed that the FEZ1 mRNA expression level was increased by 34%, 119%, 35%, and 115% after treatment with Li, VPA, CBZ, and LTG, respectively (Fig. 3A). FEZ1 was the top 5th, 141st, 193rd, and 10th most highly expressed gene among the total genes induced by Li, VPA, CBZ, and LTG, respectively (Table 1).

Table 1. The 10 most induced genes in response to each mood stabilizer

	Lithium			Valproic acid			Carbamazepine			Lamotrigine		
Rank	Symbol	Fold change	Function	Symbol	Fold change	Function	Symbol	Fold change	Function	Symbol	Fold change	Function
1	MMP14	1.40	Proteolysis	TSPAN7	5.05	Glycosylation	KIAA1033	1.91	Uncharacterized	PAIP1	2.00	RNA stabilization
2	RASIP1	1.37	Uncharacterized	CA2	3.55	One-carbon metabolism	NIPBL	1.83	Cell cycle	DNAJC10	1.87	Protein folding
3	C21orf70	1.33	Uncharacterized	LRRN3	3.33	Activation of MAPK activity	PAIP1	1.61	RNA stabilization	TUBG1	1.78	Cytoskeleton organization
4	FABP4	1.32	Proliferation	GABRB1	3.30	Ion channel complex	POLH	1.60	DNA repair	CUTA	1.76	Protein complex assembly
5	FEZ1	1.32	Cell motion/ axon guidance	GAP43	3.28	Cell motion/ axon guidance	AS3MT	1.54	Xenobiotic metabolism	KIAA1033	1.73	Uncharacterized
6	AAMP	1.31	Cell motion	ASAP3	3.20	Small GTPase signaling	ZKSCAN4	1.52	Transcription	MMP1	1.71	Proteolysis
7	LENG8	1.30	Uncharacterized	TNFAIP6	3.02	Cell adhesion	ERMN	1.52	Cytoskeleton organization	DDX59	1.70	Uncharacterized
8	MYCL1	1.30	Regulation of transcription	VGF	2.91	Cell-cell signaling	FAR1	1.50	Fatty acid metabolism	CSNK1A1	1.67	Wnt signaling
9	CRB2	1.30	Sensory perception	BIRC3	2.91	Anti-apoptosis	MAP3K2	1.50	Activation of MAPK activity	UBE4A	1.66	Proteolysis
10	NDUFB1	1.29	Oxidative phosphorylation	SPINK13	2.88	Uncharacterized	KPNA5	1.50	Intracellular protein transport	FEZ1	1.64	Cell motion/ axon guidance

The table shows the 10 most robust fold changes in the signal intensities of the mood-stabilizer-treated samples divided by the appropriate control samples. Each fold change represents the minimal value among the fold changes determined in four comparisons between duplicate mood-stabilizer-treated samples and duplicate control samples. Columns labeled *Function* indicate representative *biological process* categories from the Gene Ontology database (http://www.geneontology.org/) to which each gene belongs.

Table 2. The 10 most suppressed genes in response to each mood stabilizer

	Lithium			Valproic acid			Carbamazepine			Lamotrigine		
Rank	Symbol	Fold change	Function	Symbol	Fold change	Function	Symbol	Fold change	Function	Symbol	Fold change	Function
1	AFMID	0.63	Tryptophan metabolism	CA9	0.22	One-carbon metabolism	RBM14	0.67	Transcription	ABCD1	0.47	Fatty acid metabolism
2	RBM14	0.65	Transcription	ZP1	0.23	Fertilization	PUS1	0.71	RNA processing	NFIC	0.52	Transcription
3	RIMBP3	0.65	Uncharacterized	KCNS1	0.28	Ion transport	CLIP1	0.73	Cell cycle	PPDPF	0.59	Uncharacterized
4	RAPGEFL1	0.66	Small GTPase signaling	CHI3L2	0.31	Polysaccharide metabolism	HSP90AA1	0.74	Protein folding	ATN1	0.61	Cell death
5	SNORD14A	0.68	Uncharacterized	SERP2	0.32	Protein transport	CDK5RAP3	0.75	Cell cycle	SMARCC2	0.61	Chromatin organization
6	SETD7	0.68	Chromatin organization	OLFML3	0.33	Uncharacterized	AKIRIN1	0.76	Uncharacterized	JOSD2	0.61	Uncharacterized
7	P2RY6	0.68	Ion transport	SLC2A1	0.34	Monosaccharide transport	MAP2K3	0.76	Activation of MAPK activity	SOLH	0.61	Proteolysis
8	ZNF200	0.70	Zinc ion binding	TSPAN10	0.35	Uncharacterized	HIST2H2BF	0.77	Chromatin organization	IFITM3	0.63	Immune response
9	DOCK3	0.71	Uncharacterized	ARTN	0.35	Cell proliferation	CPT1B	0.77	Fatty acid metabolism	SLN	0.63	Calcium ion transport
10	COL4A3BP	0.72	Cell morphogenesis	C10orf10	0.35	Uncharacterized	CTSL1	0.77	Proteolysis	AHDC1	0.63	Uncharacterized

The table shows the 10 least robust fold changes in the signal intensities of the mood-stabilizer-treated samples divided by the appropriate control samples. Each fold change represents the maximal value among the fold changes determined in four comparisons between duplicate mood-stabilizer-treated samples and duplicate control samples. Columns labeled *Function* indicate representative *biological process* categories from the Gene Ontology database (http://www.geneontology.org/) to which each gene belongs.

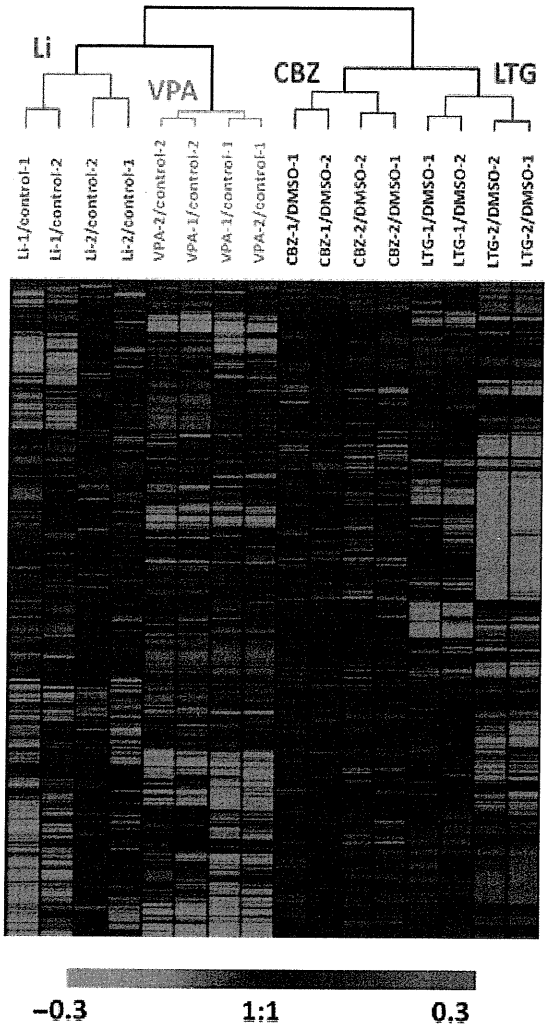

Fig. 2. Hierarchical clustering of gene expression changes caused by the mood stabilizers. Log_2-transformed ratios of the signal intensities of samples treated with mood stabilizers to the signal intensities of their controls [lithium (Li)-treated sample/non-treated control, valproic acid (VPA)-treated sample/non-treated control, carbamazepine (CBZ)-treated sample/DMSO-treated control, lamotrigine (LTG)-treated sample/DMSO-treated control] were subjected to an average linkage hierarchical clustering analysis. Ratios for each of the four combinations of duplicate drug-treated samples to their duplicate control samples were calculated.

Verification by qRT-PCR using six independent cell cultures for each mood stabilizer treatment and for the control samples showed that the FEZ1 mRNA levels were significantly increased by 49% ($p < 0.05$), 78% ($p < 0.001$), 42% ($p < 0.01$), and 47% ($p < 0.001$) following treatment with Li (0.75 mM), VPA (0.5 mM), CBZ (50 μM), and LTG (5 μM) (Fig. 3A), respectively. Western blotting analysis demonstrated that the VPA and LTG treatments significantly induced FEZ1 protein expression levels by 36% ($p < 0.05$) and 60% ($p < 0.01$), respectively, at the lower concentrations (0.5 mM and 5 μM, respectively) (Fig. 3B), while neither Li nor CBZ treatment significantly altered FEZ1 protein expression levels at lower concentrations (0.75 mM and 50 μM, respectively). On the other hand, FEZ1 protein expression levels were significantly increased by 42% ($p < 0.05$), 58% ($p < 0.05$), 75% ($p < 0.01$), and 62% ($p < 0.01$) following treatment with the higher concentrations of Li (1.2 mM), VPA (1 mM), CBZ (100 μM), and LTG (50 μM), respectively (Fig. 3C).

Suppression of RBM14 expression in human astrocytic cells

RBM14 was the only gene suppressed by all four mood stabilizers. The microarray data showed that RBM14 was decreased by 39%, 65%, 33%, and 54% following treatment with Li, VPA, CBZ, and LTG, respectively (Fig. 3D). RBM14 was the top 2nd, 808th, 1st, and 146th most robustly downregulated gene among the total genes suppressed by Li, VPA, CBZ, and LTG, respectively (Table 2). qRT-PCR analysis revealed that the mRNA levels of RBM14 were decreased by 37% ($p < 0.001$), 47% ($p < 0.05$), 32% ($p < 0.05$), and 36% ($p < 0.05$) following treatment with Li, VPA, CBZ, and LTG, respectively (Fig. 3D). However, the protein expression levels of RBM14 were not altered in response to any of the mood stabilizer treatments at any of the tested doses (Fig. 3E).

Intracellular localization of FEZ1 in human brain-derived cells

To assess FEZ1 protein expression in human brain-derived cells, the human astrocyte-derived cell line U-87 MG, the human primary astrocyte cells ACBRI 371, the human neuron-derived cell line SK-N-SH, and the human oligodendrocyte-derived cell line OL, the cultures were subjected to immunofluorescent staining with anti-FEZ1 antibody (red) and anti-GFAP (green) or anti-NeuN (green) antibodies. The cell nuclei were stained with 4′, 6-diamidino-2-phenylindole (DAPI, blue) and observed under UV excitation. The immunostaining images revealed FEZ1 protein expression in the U-87 MG (Figs. 4A–C), ACBRI 371 (Figs. 4D–F), and SK-N-SH (Figs. 4G–I) cells, but not in OL cells (data not shown). The FEZ1 immunostaining signal was localized in the cytoplasm of human astrocyte- and neuron-derived cells, while the nuclei were immunonegative (arrowheads). There were no differences in intracellular FEZ1 localization in U-87 MG cells after five days of treatment with Li, VPA, CBZ, and LTG (data not shown).

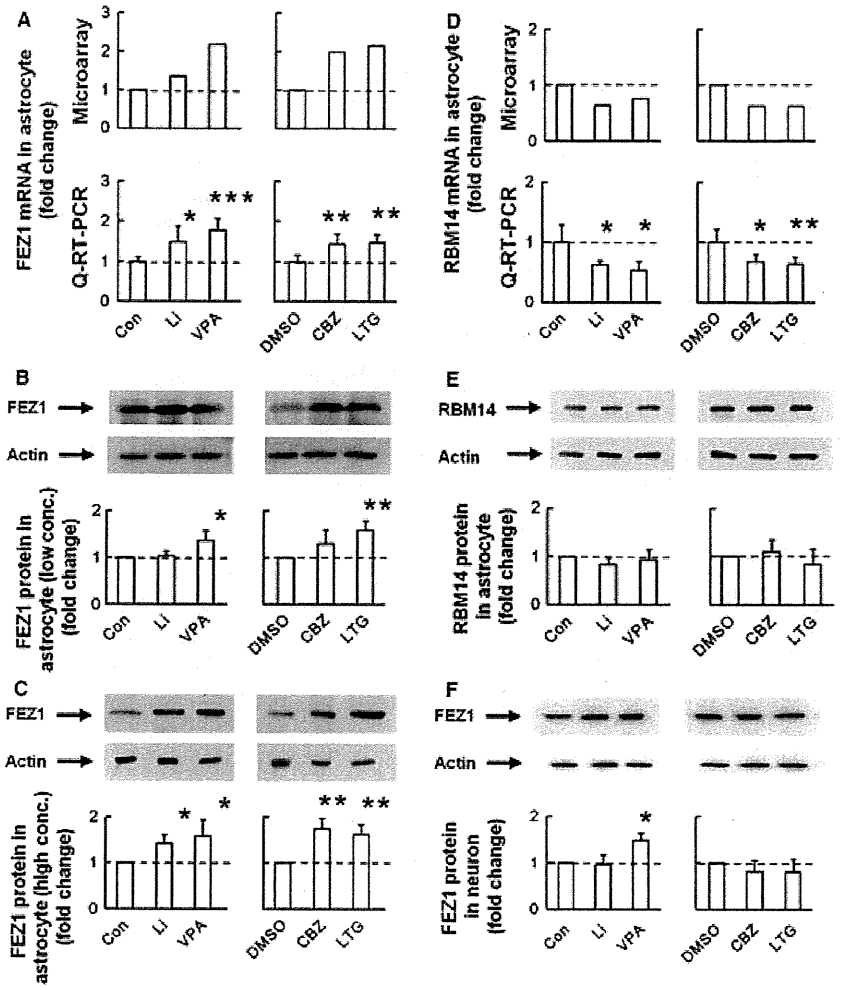

Fig. 3. Transcriptional and protein expression levels of fasciculation and elongation protein zeta 1 (FEZ1) and RNA binding motif protein 14 (RBM14) in astrocytic and neuronal cells after the mood stabilizer treatments. (**A**) The upper bar graph shows the FEZ1 transcript signal intensities determined from microarray analyses of human astrocyte-derived cells, relative to the averaged signal intensity of the control samples. The lower bar graph shows the FEZ1 transcript levels in human astrocyte-derived cells relative to the averaged signal intensity of the control samples, as measured by qRT-PCR analysis. (**B**) Gel images and bar graph of the signal intensities determined by western blotting of human astrocyte-derived cells using anti-FEZ1 antibody, after treatment with the lower concentrations of the four mood stabilizers [0.75 mM lithium (Li), 0.5 mM valproic acid (VPA), 50 μM carbamazepine (CBZ), and 5 μM lamotrigine (LTG)], relative to the averaged signal intensity of the control samples. (**C**) Gel images and bar graph of the signal intensities determined by western blotting of human astrocyte-derived cells using anti-FEZ1 antibody, after treatment with the higher concentrations of the four mood stabilizers (1.2 mM Li, 1 mM VPA, 100 μM CBZ, and 50 μM LTG), relative to the averaged signal intensity of the control samples. (**D**) The upper bar graph shows the signal intensities for the RBM14 transcript from microarray analyses of human astrocyte-derived cells relative to the averaged signal intensity of the control samples. The lower bar graph shows the transcript levels of RBM14 in human astrocyte-derived cells relative to the averaged signal intensity of the control samples, as measured by qRT-PCR analysis. (**E**) Gel images and bar graph of the signal intensities determined by western blotting of human astrocyte-derived cells using anti-RBM14 antibody, after treatment with the higher concentrations of the four mood stabilizers (1.2 mM Li, 1 mM VPA, 100 μM CBZ, and 50 μM LTG), relative to the averaged signal intensity of the control samples. (**F**) Gel images and bar graph of the signal intensities determined by western blotting of human neuron-derived cells using anti-FEZ1 antibody, after treatment with the higher concentrations of the four mood stabilizers (1.2 mM Li, 1 mM VPA, 100 μM CBZ, and 50 μM LTG), relative to the averaged signal intensity of the control samples. Con = non-treated control; DMSO = dimethyl sulfoxide-treated control. *$p < 0.05$; **$p < 0.01$; ***$p < 0.001$.

Effect of mood stabilizers on FEZ1 expression in human neuronal cells

To determine whether any of the mood stabilizers affected FEZ1 protein expression levels in human neuron-derived cells, human neuron-derived SK-N-SH cells were subjected to mood stabilizer treatments in the same manner employed for the U-87 MG experiments. Treatments with any of the four mood stabilizers at the lower

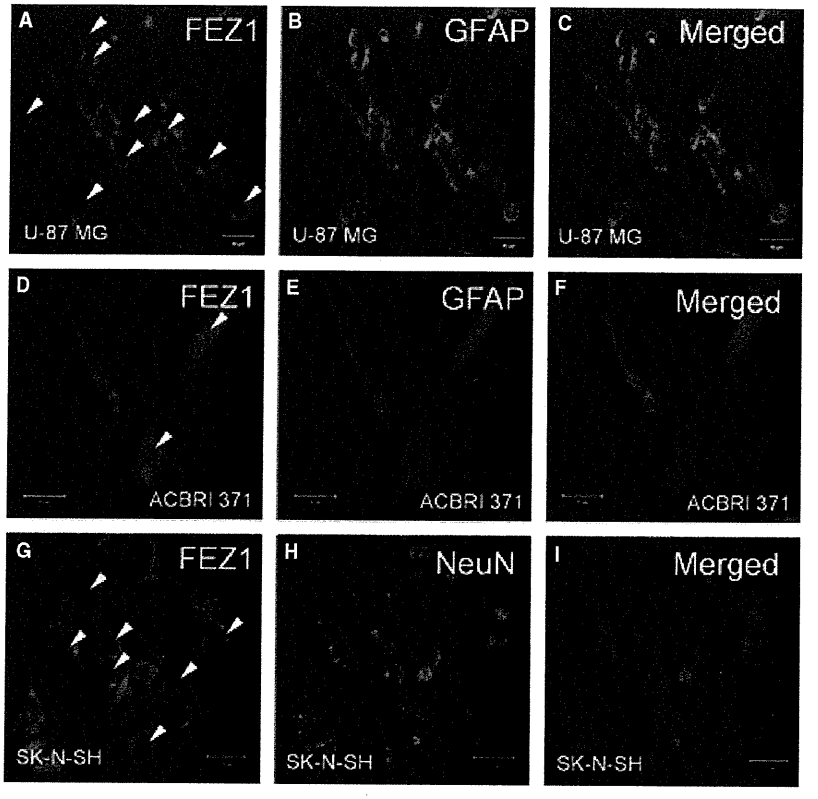

Fig. 4. Intracellular localization of fasciculation and elongation protein zeta 1 (FEZ1) protein in human astrocytic and neuronal cells. Figures A, B, and C show the intracellular localization of FEZ1 protein (**A**), glial fibrillary acidic protein (GFAP), an astrocyte marker (**B**), and the merged image showing the distribution of FEZ1 and GFAP (**C**) in the human astrocyte-derived cell line U-87 MG (scale bar: 40 μm). D, E, and F show the intracellular localization of FEZ1 protein (**D**), GFAP protein (**E**), and the merged image showing the distribution of FEZ1 and GFAP (**F**) in the human primary astrocyte cell culture ACBRI371 (scale bar: 40 μm). Figures G, H, and I show the intracellular localization of FEZ1 protein (**G**), the neuronal specific nuclear protein (NeuN) (**H**), and the merged image showing the distribution of FEZ1 and NeuN (**I**) in the human neuron-derived cell line SK-N-SH (scale bar: 20 μm). Cell nuclei were stained with 4′,6-diamidino-2-phenylindole (DAPI, blue) (C, F, I). Arrow heads indicate nuclei of cells lacking FEZ1 signal.

concentrations did not alter FEZ1 protein expression levels in SK-N-SH cells (data not shown). Following treatment with the mood stabilizers at the high concentrations, only VPA increased the FEZ1 protein expression level in SK-N-SH cells (Fig. 3F).

Discussion

Among the four mood stabilizers, VPA affected the expression of the largest numbers of genes. VPA may exert its effect on transcriptional regulation by inhibiting histone deacetylase (HDAC) activity (33, 34); however, it remains uncertain whether the strong effect of VPA on transcriptional regulation is relevant to its mood-stabilizing effect and/or HDAC inhibition-mediated teratogenesis (35). It is interesting that LTG also affects a relatively large number of genes, despite the use of a concentration of LTG in the microarray experiments that was close to the lower limit of its therapeutic range (36, 37). LTG may have unknown mechanisms of action that are relevant to its potent effect on transcriptional regulation.

The clustering analysis suggested that Li and VPA regulated the transcriptional activities of a common set of genes, whereas CBZ with LTG affected a different set of genes. Li and VPA have been reported to share common molecular mechanisms of action, including effects on glycogen synthase kinase 3β (38, 39) and phosphatidylinositol (40) signaling, which may underlie the common effects of Li and VPA on transcriptional regulation in U-87 MG cells. CBZ and LTG may share other unknown mechanisms which cause the observed transcriptional alterations in astrocytes.

Interestingly, only VPA increased FEZ1 protein expression in a neuron-derived cell line at a concentration representing the higher limit of the therapeutic range, while Li, CBZ, and LTG did not induce FEZ1 protein expression in neuronal cells at any concentration. The FEZ1 gene has been functionally characterized in the rodent brain and

a human neuron-derived cell line (41). These rodent studies have indicated that FEZ1 is preferentially expressed in neuronal cells and involved in normal axonal bundling, elongation within axon bundles of neurons, transport of intracellular components (including mitochondria), and release of neurotransmitters (32, 42, 43). FEZ1 protein is phosphorylated by PKCζ and then translocated from the cytoplasmic membrane to the cytoplasm, where it induces axonal growth and neuronal differentiation (44). FEZ1 protein has also been reported to localize to growth cones and associate with F-actin in SK-N-SH cells and cultured hippocampal neurons (41). Although the mechanism underlying its transcriptional regulation requires further investigation, induction of FEZ1 protein in neuronal cells by VPA might contribute to axonal bundling, transport of intracellular components, and neurotransmitter release.

The most intriguing finding of the genome-wide expression analysis of mood-stabilizer-treated U-87 MG cells was that only the FEZ1 and RBM14 transcripts were substantially induced and suppressed by all four mood stabilizers. The significant induction of FEZ1 molecules at both the transcript and the protein levels was verified by qRT-PCR and western blotting. Although FEZ1 transcript levels were significantly increased by the four mood stabilizers at lower concentrations, protein levels increased only at higher Li and CBZ concentrations. In general, changes in protein levels depend on levels of the transcript, translation efficiency, and degradation of the existing protein (45). Although the modest increase in FEZ1 transcripts after Li and CBZ treatments at lower concentrations may not be sufficient to yield a corresponding increase in FEZ1 translation, it implies that higher doses of Li and CBZ may increase transcript levels to a degree that allows for increased FEZ1 translation. Mood stabilizers might somehow affect translation efficiency and degradation of the existing protein as well, although these possibilities were not addressed in this study.

In addition to neuronal cells, FEZ1 is expressed in cultured rat neonatal astrocytes (46); however, it is expressed at barely detectable levels in adult astrocytes and oligodendrocytes (32). In our experiments, unlike the previous adult rodent studies, FEZ1 protein was expressed in the cytoplasm of both transformed and primary astrocytes, as well as in neuronal cells from the human adult brain, while it was not detectable in the human oligodendrocyte cell line (data not shown). No differences were detected in the intracellular distribution pattern of the FEZ1 protein between the human astrocytic and neuronal cells.

In general, the transcription of genes in certain cell types can vary among species. One example of this is the transcriptional regulation of toll-like receptors and nitric oxide synthase 2 in humans and rodents (47, 48). While exons 2-10 of human FEZ1 and rodent Fez1 are highly homologous (mouse: 90%, rat: 91%), exon 1 and the promoter region are not. This difference in the promoter region may underlie the expression of the gene in human astrocytes, but its absence in rodents.

Astrocytes are compact round cells in the early developmental stages, and subsequently, they project highly branched cellular processes that form connections with other cell types or with brain structures, similar to the extension of axons and dendrites observed in neurons. The localization of FEZ1 proteins suggests that FEZ1 may be involved in the extension and maintenance of astrocyte processes, mitochondrial functions, and the development and maintenance of structural formations in astrocytes; however, the function of FEZ1 protein in astrocytes requires further investigation.

Although there are reports that FEZ1 transcripts are decreased in postmortem brain tissue of patients with schizophrenia (49) and that FEZ1 and schizophrenia are modestly associated (50), neither postmortem brain studies nor genetic association studies targeting FEZ1 have been reported. However, indirect evidence from animal models and cell culture studies suggests the possible involvement of FEZ1 dysfunction in the pathogenesis of BD. To this end, FEZ1 knockout mice are hypersensitive to psychostimulant treatment (51), which suggests that hypofunction of FEZ1 may contribute to hyperdopaminergic conditions which have been implicated in the pathogenesis of the manic state of BD (52). In addition, FEZ1 has been reported to play an important role in the establishment of neuronal polarity by controlling the axonal transport of mitochondria (53, 54). Thus, an impairment of FEZ1 might be involved in the mitochondrial dysfunction implicated in BD (55, 56). Further studies will be needed to investigate abnormalities in FEZ1 expression and function in postmortem brains of BD subjects.

Our finding that four widely prescribed mood stabilizers commonly induced FEZ1 protein expression in astrocyte-derived cells raises the question of what the link is between the mechanisms of action of the mood stabilizers and FEZ1 induction. It is also unclear whether FEZ1 induction is specific to these mood stabilizers, and whether this induction is involved in the mood-stabilizing effects of these drugs. Further studies

will be needed to address these issues and the involvement of FEZ1 in the pathogenesis of BD.

Although the RBM14 transcript was suppressed by the mood stabilizer treatments, RBM14 protein expression was not affected by any of the mood stabilizers. While protein levels generally correlate with transcript levels, there can be discrepancies due to variability in translation efficiency and protein degradation (45). Thus, RBM14 translation efficiency may have increased or RBM14 degradation may have decreased in parallel with the decrease in RBM14 transcripts. Since RBM14 exerts its cellular effects by encoding the coactivator activator (CoAA) protein (57), the suppression of RBM14 transcripts may not be directly relevant to the mechanism of action of mood stabilizers. However, there remains the possibility that decreases in RBM14 transcripts may influence cellular function by modulating the expression of other transcripts.

Besides the genes commonly altered by the four mood stabilizers, each mood stabilizer uniquely altered the expression of certain genes with robust fold changes as shown in Tables 1 and 2. Although further studies will be needed to characterize the function of these regulated genes and their roles in mood stabilization, previous studies have suggested the possible involvement of some of these genes in the mechanism of action of the respective mood stabilizer. For example, VPA induced gamma-aminobutyric acid A receptor, beta 1 (GABRB1) and growth associated protein 43 (GAP43) transcripts by 330% and 328%, respectively (Table 1). GABA A receptor is expressed in both astrocytes and neurons. The GABA A receptor is thought to transfer signals from inhibitory interneurons to adjacent glial cells, and may regulate extracellular Cl^- concentrations in the vicinity of a GABAergic synapse (58). The SPECT study showed that levels of GABA A receptors were decreased in the sensory motor cortex of mood disorder patients with akinetic catatonia (59), whereas GABA receptors were increased in the rodent hippocampus after VPA treatment (60). These disease-related or VPA-induced alterations in GABA receptor expression may, at least in part, reflect the expression of GABA A receptors in astrocytes.

VPA was previously reported to increase neuronal GAP43 and cell survival *in vitro* (61). The present study demonstrated that VPA also induces GAP43 in astrocytes. Although GAP43 is a calmodulin-binding phosphoprotein primarily found in neuronal growth cones and is an intrinsic presynaptic determinant for neurite outgrowth and plasticity (62), it is also expressed in astrocytes, in particular type 2 astrocytes (63, 64). One study reported that ischemic injury induces GAP43 expression in reactive astrocytes, which protect the brain from ischemic injury by normalizing extracellular fluid H^+ or glutamate levels, or by releasing neuronal growth factors (65, 66). Given that postmortem brain studies have shown that GAP43 expression is significantly reduced in the anterior cingulate cortex of BD patients (67) and the prefrontal cortex of depressed suicide victims (68), VPA might exert its effects by inducing GAP43 levels.

DNA polymerase eta (POLH) increased by 60% after CBZ treatment, whereas interferon-induced transmembrane protein 3 (IFITM3) decreased by 37% after LTG treatment (Tables 1 and 2). Postmortem brain microarray analyses showed that POLH expression was decreased in the hippocampal CA1 region (69), and IFITM3 was increased in the prefrontal cortex of BD patients (70). This suggests the possibility that CBZ-induced POLH expression and LTG-mediated IFITM3 suppression may normalize the altered levels of these genes in affected brains. Thus, transcriptional regulation may underlie the mood-stabilizing actions of these drugs.

In conclusion, the microarray data obtained for human astrocytic cells identified FEZ1 as a gene that is commonly induced by the four mood stabilizers, Li, VPA, CBZ, and LTG. Unlike the studies performed in rodents, in the present study FEZ1 was expressed in the cytoplasm of human astrocytic cells and neuronal cells. Our data suggest that FEZ1 may play important roles in human astrocytes, and that mood stabilizers might exert their cytoprotective and mood-stabilizing effects via FEZ1 induction in astrocytes. Further studies will be needed to address the involvement of FEZ1 in the mechanisms of action of mood stabilizers and the pathogenesis of BD.

Acknowledgements

This work was supported by a grant-in-aid for scientific research (B) (no. 19390300) from the Ministry of Education, Culture, Sports, Science, and Technology of Japan, a grant-in-aid from the Japan Research Foundation for Clinical Pharmacology, and the Intramural Research Grant (21-6) for Neurological and Psychiatric Disorders from the National Center of Neurology and Psychiatry. We appreciate the assistance of Ms. Yoshie Kikuchi (Tohoku University) for the technical contributions in cell culture and qRT-PCR experiments.

References

1. Williams R, Ryves WJ, Dalton EC et al. A molecular cell biology of lithium. Biochem Soc Trans 2004; 32: 799–802.

2. Di Daniel E, Cheng L, Maycox PR, Mudge AW. The common inositol-reversible effect of mood stabilizers on neurons does not involve GSK3 inhibition, myo-inositol-1-phosphate synthase or the sodium-dependent myo-inositol transporters. Mol Cell Neurosci 2006; 32: 27–36.
3. Beaulieu JM, Caron MG. Looking at lithium: molecular moods and complex behaviour. Mol Interv 2008; 8: 230–241.
4. O'Brien WT, Klein PS. Validating GSK3 as an in vivo target of lithium action. Biochem Soc Trans 2009; 37: 1133–1138.
5. Quiroz JA, Gould TD, Manji HK. Molecular effects of lithium. Mol Interv 2004; 4: 259–272.
6. Shaltiel G, Dalton EC, Belmaker RH, Harwood AJ, Agam G. Specificity of mood stabilizer action on neuronal growth cones. Bipolar Disord 2007; 9: 281–289.
7. Leng Y, Liang MH, Ren M, Marinova Z, Leeds P, Chuang DM. Synergistic neuroprotective effects of lithium and valproic acid or other histone deacetylase inhibitors in neurons: roles of glycogen synthase kinase-3 inhibition. J Neurosci 2008; 28: 2576–2588.
8. Du J, Gray NA, Falke C, Yuan P, Szabo S, Manji HK. Structurally dissimilar antimanic agents modulate synaptic plasticity by regulating AMPA glutamate receptor subunit GluR1 synaptic expression. Ann NY Acad Sci 2003; 1003: 378–380.
9. Friedrich MJ. Molecular studies probe bipolar disorder. JAMA 2005; 293: 535–536.
10. Doetsch F, Caillé I, Lim DA, García-Verdugo JM, Alvarez-Buylla A. Subventricular zone astrocytes are neural stem cells in the adult mammalian brain. Cell 1999; 97: 703–716.
11. Hama K, Arii T, Kosaka T. Three-dimensional organization of neuronal and glial processes: high voltage electron microscopy. Microsc Res Tech 1994; 29: 357–367.
12. Haydon PG. GLIA: listening and talking to the synapse. Nat Rev Neurosci 2001; 2: 185–193.
13. Kosaka T, Hama K. Three-dimensional structure of astrocytes in the rat dentate gyrus. J Comp Neurol 1986; 249: 242–260.
14. Ventura R, Harris KM. Three-dimensional relationships between hippocampal synapses and astrocytes. J Neurosci 1999; 19: 6897–6906.
15. Rajkowska G. Cell pathology in bipolar disorder. Bipolar Disord 2002; 4: 105–116.
16. Ongür D, Drevets WC, Price JL. Glial reduction in the subgenual prefrontal cortex in mood disorders. Proc Natl Acad Sci USA 1998; 95: 13290–13295.
17. Rajkowska G, Halaris A, Selemon LD. Reductions in neuronal and glial density characterize the dorsolateral prefrontal cortex in bipolar disorder. Biol Psychiatry 2001; 49: 741–752.
18. Manji HK, Moore GJ, Rajkowska G, Chen G. Neuroplasticity and cellular resilience in mood disorders. Mol Psychiatry 2000; 5: 578–593.
19. Webster MJ, O'Grady J, Kleinman JE, Weickert CS. Glial fibrillary acidic protein mRNA levels in the cingulate cortex of individuals with depression, bipolar disorder and schizophrenia. Neuroscience 2005; 133: 453–461.
20. Johnston-Wilson NL, Sims CD, Hofmann JP et al. Disease-specific alterations in frontal cortex brain proteins in schizophrenia, bipolar disorder, and major depressive disorder. The Stanley Neuropathology Consortium. Mol Psychiatry 2000; 5: 142–149.
21. Andreazza AC, Cassini C, Rosa AR et al. Serum S100B and antioxidant enzymes in bipolar patients. J Psychiatr Res 2007; 41: 523–529.
22. Roche S, Cassidy F, Zhao C et al. Candidate gene analysis of 21q22: support for S100B as a susceptibility gene for bipolar affective disorder with psychosis. Am J Med Genet B Neuropsychiatr Genet 2007; 144B: 1094–1096.
23. Pardo R, Andreolotti AG, Ramos B, Picatoste F, Claro E. Opposed effects of lithium on the MEK-ERK pathway in neural cells: inhibition in astrocytes and stimulation in neurons by GSK3 independent mechanisms. J Neurochem 2003; 87: 417–426.
24. Chen PS, Peng GS, Li G et al. Valproate protects dopaminergic neurons in midbrain neuron/glia cultures by stimulating the release of neurotrophic factors from astrocytes. Mol Psychiatry 2006; 11: 1116–1125.
25. Lubrich B, van Calker D. Inhibition of the high affinity myo-inositol transport system: a common mechanism of action of antibipolar drugs? Neuropsychopharmacology 1999; 21: 519–529.
26. Li B, Zhang S, Li M, Zhang H, Hertz L, Peng L. Down-regulation of GluK2 kainate receptor expression by chronic treatment with mood-stabilizing anti-convulsants or lithium in cultured astrocytes and brain, but not in neurons. Neuropharmacology 2009; 57: 375–385.
27. Li B, Zhang S, Li M, Hertz L, Peng L. Chronic treatment of astrocytes with therapeutically relevant fluoxetine concentrations enhances cPLA2 expression secondary to 5-HT2B-induced, transactivation-mediated ERK1/2 phosphorylation. Psychopharmacology 2009; 207: 1–12.
28. Song D, Du T, Li B et al. Astrocytic alkalinization by therapeutically relevant lithium concentrations: implications for myo-inositol depletion. Psychopharmacology 2008; 200: 187–195.
29. Dahlquist KD, Salomonis N, Vranizan K, Lawlor SC, Conklin BR. GenMAPP, a new tool for viewing and analyzing microarray data on biological pathways. Nat Genet 2002; 31: 19–20.
30. Miller LD, Long PM, Wong L, Mukherjee S, McShane LM, Liu ET. Optimal gene expression analysis by microarrays. Cancer Cell 2002; 2: 353–361.
31. Choe SE, Boutros M, Michelson AM, Church GM, Halfon MS. Preferred analysis methods for Affymetrix GeneChips revealed by a wholly defined control dataset. Genome Biol 2005; 6: R16.
32. Honda A, Miyoshi K, Baba K et al. Expression of fasciculation and elongation protein zeta-1 (FEZ1) in the developing rat brain. Brain Res Mol Brain Res 2004; 122: 89–92.
33. Busa WB, Gimlich RL. Lithium-induced teratogenesis in frog embryos prevented by a polyphosphoinositide cycle intermediate or a diacylglycerol analog. Dev Biol 1989; 132: 315–324.
34. Phiel CJ, Zhang F, Huang EY, Guenther MG, Lazar MA, Klein PS. Histone deacetylase is a direct target of valproic acid, a potent anticonvulsant, mood stabilizer, and teratogen. J Biol Chem 2001; 276: 36734–36741.
35. Gurvich N, Berman MG, Wittner BS, Gentleman RC, Klein PS, Green JB. Association of valproate-induced teratogenesis with histone deacetylase inhibition in vivo. FASEB J 2005; 19: 1166–1168.
36. May TW, Rambeck B, Jurgens U. Serum concentrations of lamotrigine in epileptic patients: the influence of dose and comedication. Ther Drug Monit 1996; 18: 523–531.
37. Fraser AD, MacNeil W, Isner AF, Camfield PR. Lamotrigine analysis in serum by high-performance liquid chromatography. Ther Drug Monit 1995; 17: 174–178.
38. Chen G, Huang LD, Jiang YM, Manji HK. The mood-stabilizing agent valproate inhibits the activity of glycogen synthase kinase-3. J Neurochem 1999; 72: 1327–1330.

39. De Sarno P, Li X, Jope RS. Regulation of Akt and glycogen synthase kinase-3 beta phosphorylation by sodium valproate and lithium. Neuropharmacology 2002; 43: 1158–1164.
40. Williams RS, Cheng L, Mudge AW, Harwood AJ. A common mechanism of action for three mood-stabilizing drugs. Nature 2002; 417: 292–295.
41. Miyoshi K, Honda A, Baba K et al. Disrupted-In-Schizophrenia 1, a candidate gene for schizophrenia, participates in neurite outgrowth. Mol Psychiatry 2003; 8: 685–694.
42. Bloom L, Horvitz HR. The Caenorhabditis elegans gene unc-76 and its human homologs define a new gene family involved in axonal outgrowth and fasciculation. Proc Natl Acad Sci USA 1997; 94: 3414–3419.
43. Assmann EM, Alborghetti MR, Camargo ME, Kobarg J. FEZ1 dimerization and interaction with transcription regulatory proteins involves its coiled-coil region. J Biol Chem 2006; 281: 9869–9881.
44. Kuroda S, Nakagawa N, Tokunaga C, Tatematsu K, Tanizawa K. Mammalian homologue of the Caenorhabditis elegans UNC-76 protein involved in axonal outgrowth is a protein kinase C zeta-interacting protein. J Cell Biol 1999; 144: 403–411.
45. de Sousa Abreu R, Penalva LO, Marcotte EM, Vogel C. Global signatures of protein and mRNA expression levels. Mol Biosyst 2009; 5: 1512–1526.
46. He J, Liu J, Zhang Z, Sun M, Zhu T, Xia C. Expression of fasciculation and elongation protein zeta-1 (FEZ1) in cultured rat neonatal astrocytes. Mol Cell Biochem 2009; 325: 159–167.
47. Rehli M. Of mice and men: species variations of Toll-like receptor expression. Trends Immunol 2002; 23: 375–378.
48. Rico D, Vaquerizas JM, Dopazo H, Bosca L. Identification of conserved domains in the promoter regions of nitric oxide synthase 2: implications for the species-specific transcription and evolutionary differences. BMC Genomics 2007; 8: 271.
49. Lipska BK, Peters T, Hyde TM et al. Expression of DISC1 binding partners is reduced in schizophrenia and associated with DISC1 SNPs. Hum Mol Genet 2006; 15: 1245–1258.
50. Yamada K, Nakamura K, Minabe Y et al. Association analysis of FEZ1 variants with schizophrenia in Japanese cohorts. Biol Psychiatry 2004; 56: 683–690.
51. Sakae N, Yamasaki N, Kitaichi K et al. Mice lacking the schizophrenia-associated protein FEZ1 manifest hyperactivity and enhanced responsiveness to psychostimulants. Hum Mol Genet 2008; 17: 3191–3203.
52. Cousins DA, Butts K, Young AH. The role of dopamine in bipolar disorder. Bipolar Disord 2009; 11: 787–806.
53. Fujita T, Maturana AD, Ikuta J et al. Axonal guidance protein FEZ1 associates with tubulin and kinesin motor protein to transport mitochondria in neurites of NGF-stimulated PC12 cells. Biochem Biophys Res Commun 2007; 361: 605–610.
54. Ikuta J, Maturana A, Fujita T et al. Fasciculation and elongation protein zeta-1 (FEZ1) participates in the polarization of hippocampal neuron by controlling the mitochondrial motility. Biochem Biophys Res Commun 2007; 353: 127–132.
55. Kato T. The role of mitochondrial dysfunction in bipolar disorder. Drug News Perspect 2006; 19: 597–602.
56. Quiroz JA, Gray NA, Kato T, Manji HK. Mitochondrially mediated plasticity in the pathophysiology and treatment of bipolar disorder. Neuropsychopharmacology 2008; 33: 2551–2565.
57. Auboeuf D, Dowhan DH, Li X et al. CoAA, a nuclear receptor coactivator protein at the interface of transcriptional coactivation and RNA splicing. Mol Cell Biol 2004; 24: 442–453.
58. MacVicar BA, Tse FW, Crichton SA, Kettenmann H. GABA-activated Cl- channels in astrocytes of hippocampal slices. J Neurosci 1989; 9: 3577–3583.
59. Northoff G, Steinke R, Czcervenka C et al. Decreased density of GABA-A receptors in the left sensorimotor cortex in akinetic catatonia: investigation of in vivo benzodiazepine receptor binding. J Neurol Neurosurg Psychiatry 1999; 67: 445–450.
60. Motohashi N. GABA receptor alterations after chronic lithium administration. Comparison with carbamazepine and sodium valproate. Prog Neuropsychopharmacol Biol Psychiatry 1992; 16: 571–579.
61. Yuan PX, Huang LD, Jiang YM, Gutkind JS, Manji HK, Chen G. The mood stabilizer valproic acid activates mitogen-activated protein kinases and promotes neurite growth. J Biol Chem 2001; 276: 31674–31683.
62. Aigner L, Arber S, Kapfhammer JP et al. Overexpression of the neural growth-associated protein GAP-43 induces nerve sprouting in the adult nervous system of transgenic mice. Cell 1995; 83: 269–278.
63. da Cunha A, Vitković L. Regulation of immunoreactive GAP-43 expression in rat cortical macroglia is cell type specific. J Cell Biol 1990; 111: 209–215.
64. Vitković L, Steisslinger HW, Aloyo VJ, Mersel M. The 43-kDa neuronal growth-associated protein (GAP-43) is present in plasma membranes of rat astrocytes. Proc Natl Acad Sci USA 1988; 85: 8296–8300.
65. Yamada K, Goto S, Oyama T, Inoue N, Nagahiro S, Ushio Y. In vivo induction of the growth associated protein GAP43/B-50 in rat astrocytes following transient middle cerebral artery occlusion. Acta Neuropathol 1994; 88: 553–557.
66. Petito CK, Chung M, Halaby IA, Cooper AJ. Influence of the neuronal environment on the pattern of reactive astrocytosis following cerebral ischemia. Prog Brain Res 1992; 94: 381–387.
67. Eastwood SL, Harrison PJ. Synaptic pathology in the anterior cingulate cortex in schizophrenia and mood disorders. A review and a Western blot study of synaptophysin, GAP-43 and the complexins. Brain Res Bull 2001; 55: 569–578.
68. Hrdina P, Faludi G, Li Q et al. Growth-associated protein (GAP-43), its mRNA, and protein kinase C (PKC) isoenzymes in brain regions of depressed suicides. Mol Psychiatry 1998; 3: 411–418.
69. Benes FM, Lim B, Subburaju S. Site-specific regulation of cell cycle and DNA repair in post-mitotic GABA cells in schizophrenic versus bipolars. Proc Natl Acad Sci USA 2009; 106: 11731–11736.
70. Iwamoto K, Kakiuchi C, Bundo M, Ikeda K, Kato T. Molecular characterization of bipolar disorder by comparing gene expression profiles of postmortem brains of major mental disorders. Mol Psychiatry 2004; 9: 406–416.

CLINICAL REPORT

AMERICAN JOURNAL OF medical genetics PART A

A De Novo Deletion of 20q11.2–q12 in a Boy Presenting With Abnormal Hands and Feet, Retinal Dysplasia, and Intractable Feeding Difficulty

Yoko Hiraki,[1,2] Akira Nishimura,[2] Michiko Hayashidani,[3] Yoshiko Terada,[4] Gen Nishimura,[5] Nobuhiko Okamoto,[6] Sachiko Nishina,[7] Yoshinori Tsurusaki,[2] Hiroshi Doi,[2] Hirotomo Saitsu,[2] Noriko Miyake,[2] and Naomichi Matsumoto[2]*

[1]Hiroshima Municipal Center for Child Health and Development, Hiroshima, Japan

[2]Department of Human Genetics, Yokohama City University Graduate School of Medicine, Yokohama, Japan

[3]Medical Center for Premature and Neonatal Infants, Hiroshima City Hospital, Hiroshima, Japan

[4]Department of Ophthalmology, Hiroshima City Hospital, Hiroshima, Japan

[5]Department of Pediatric Imaging, Tokyo Metropolitan Children's Medical Center, Tokyo, Japan

[6]Department of Medical Genetics, Osaka Medical Center and Research Institute for Maternal and Child Health, Osaka, Japan

[7]Department of Ophthalmology, National Center for Child Health and Development, Tokyo, Japan

Received 18 June 2010; Accepted 23 October 2010

Proximal interstitial deletions involving 20q11–q12 are very rare. Only two cases have been reported. We describe another patient with 20q11.21–q12 deletion. We precisely mapped the 6.5-Mb deletion and successfully determined the deletion landmarks at the nucleotide level. Common clinical features among the three cases include developmental delay, intractable feeding difficulties with gastroesophageal reflux, and facial dysmorphism including triangular face, hypertelorism, and hypoplastic alae nasi, indicating that the 20q11.2–q12 deletion can be a clinically recognizable syndrome. This is also supported by the fact that the three deletions overlap significantly. In addition, unique features such as arthrogryposis/fetal akinesia (hypokinesia) deformation and retinal dysplasia are recognized in the patient reported herein.

Key words: 20q interstitial deletion; abnormal hands and feet; retinal dysplasia; feeding difficulty

How to Cite this Article:
Hiraki Y, Nishimura A, Hayashidani M, Terada Y, Nishimura G, Okamoto N, Nishina S, Tsurusaki Y, Doi H, Saitsu H, Miyake N, Matsumoto N. 2011. A de novo deletion of 20q11.2–q12 in a boy presenting with abnormal hands and feet, retinal dysplasia, and intractable feeding difficulty.
Am J Med Genet Part A 155:409–414.

INTRODUCTION

Interstitial deletions of the long arm of chromosome 20 are rare. To our knowledge, a total of 12 patients have been reported in the literature [Petersen et al., 1987; Shabtai et al., 1993; Aldred et al., 2002; Genevieve et al., 2005; Callier et al., 2006; Borozdin et al., 2007; Iqbal and Al-Owain, 2007]. Among them, only two cases showed the proximal q deletion (20q11–q12), not extending to q13 [Callier et al., 2006; Iqbal and Al-Owain, 2007]. One patient had a 6.6-Mb deletion at 20q11.21–q11.23 [Callier et al., 2006], and the other [Iqbal and Al-Owain, 2007] showed a 6.8-Mb deletion at 20q11.2–q12. Here, we report on the third patient with a 6.5-Mb deletion at 20q11.21–q12, clinically showing mental retardation, minor craniofacial anomalies, and intractable feeding difficulties. The deletion has been precisely analyzed at the nucleotide level and his detailed clinical manifestations will be presented.

Grant sponsor: Japan Society for the Promotion of Science (JSPS); Grant sponsor: Ministry of Health, Labour and Welfare; Grant sponsor: Ministry of Education, Culture, Sports, Science and Technology of Japan; Grant sponsor: Scientific Research.
*Correspondence to:
Naomichi Matsumoto, Department of Human Genetics, Yokohama City University Graduate School of Medicine, Fukuura 3-9, Kanazawa-ku, Yokohama 236-0004, Japan. E-mail: naomat@yokohama-cu.ac.jp
Published online 11 January 2011 in Wiley Online Library (wileyonlinelibrary.com).
DOI 10.1002/ajmg.a.33818

CLINICAL REPORT

The 18-month-old boy was the first product of healthy 22-year-old mother and 25-year-old father without any consanguinity. Pregnancy was uneventful. Family history was unremarkable. He was born by spontaneous vaginal delivery at 38 weeks of gestation. Birth weight was 2,230 g (−1.7 SD), length 44.0 cm (−1.9 SD), and OFC 32.5 cm (−0.3 SD). Multiple malformations including patent ductus arteriosus, patency of foramen ovale, and dysmorphic face were noted. He was tube-fed due to poor swallowing and oxygen therapy was required until 4 months because of respiratory disturbance. X-ray examination at age of 1 month revealed small thorax and mild slender long bones. In addition, right eye retinal fold was pointed out. At age of 3 months, upper gastrointestinal tract was investigated because of recurrent vomiting, and gastroesophageal reflux (GER) and esophageal hiatus hernia were found. Esophageal hiatus hernia was alleviated spontaneously, but GER persisted.

At age of 4 months, he was referred to us for evaluation of his developmental delay. He was noted to have the following craniofacial features: triangular face, premature closure fontanelle, slopping forehead, wide bending eyebrows, hypertelorism, low-set and posterior rotated ears, long columella nasi, mild hypoplastic alae nasi, short and well-defined philtrum, thin lips with tucked-in lower lip, submucosal cleft palate, microretrognathia and posterior low hair-line (Fig. 1A,B and Table I). Additionally, abnormal hands and feet were recognized, consisted of restriction of all proximal interphalangeal joints and over-extension of all distal interphalangeal joints of hands and feet, radial deviation of 2nd fingers, clinodactyly of the 2nd and 5th fingers, lack of flexion creases bilaterally, right preaxial polydactyly, left single palmar, and talipes valgus. Mild restriction of elbow, hip and knee joints bilaterally was also noted (Fig. 1C–E and Table I).

At 15 months, his weight was 7.5 kg (−2.3 SD), length 71.8 cm (−2.7 SD), and OFC 44.4 cm (−1.6 SD). He could roll over one side and shift a toy from one hand to the other. Social smile was seen, but he could not recognize his parents (DQ 48). His dysphagia persisted based on the modified swallowing study [Kanda et al., 2005]; he required tube-feeding, and rejected oral intake. Ophthalmic examination at 15 months revealed broom-like pattern of retinal vessels extending from optic disc to periphery with a falciform retinal fold in the right eye, causing visual impairment. In the left eye, mild opacity in the lateral portion of vitreous body was found. These findings led to the diagnosis of bilateral retinal dysplasia. Anterior segment and optic disc were normal. Left hearing loss was suspected by auditory brainstem response, otoacoustic emission, and behavioral observation audiometry. Brain magnetic resonance imaging revealed cortical atrophy and mild ventriculomegaly. Blood biochemistry and abdominal ultrasonographic examination were all normal. Serological TORCH (toxoplasma, rubella, cytomegarovirus, and herpes simplex) testing was negative. At 18 months, the shortening of 5th middle phalanges of fingers and absence of middle phalanges of the toes were confirmed by X-ray examination.

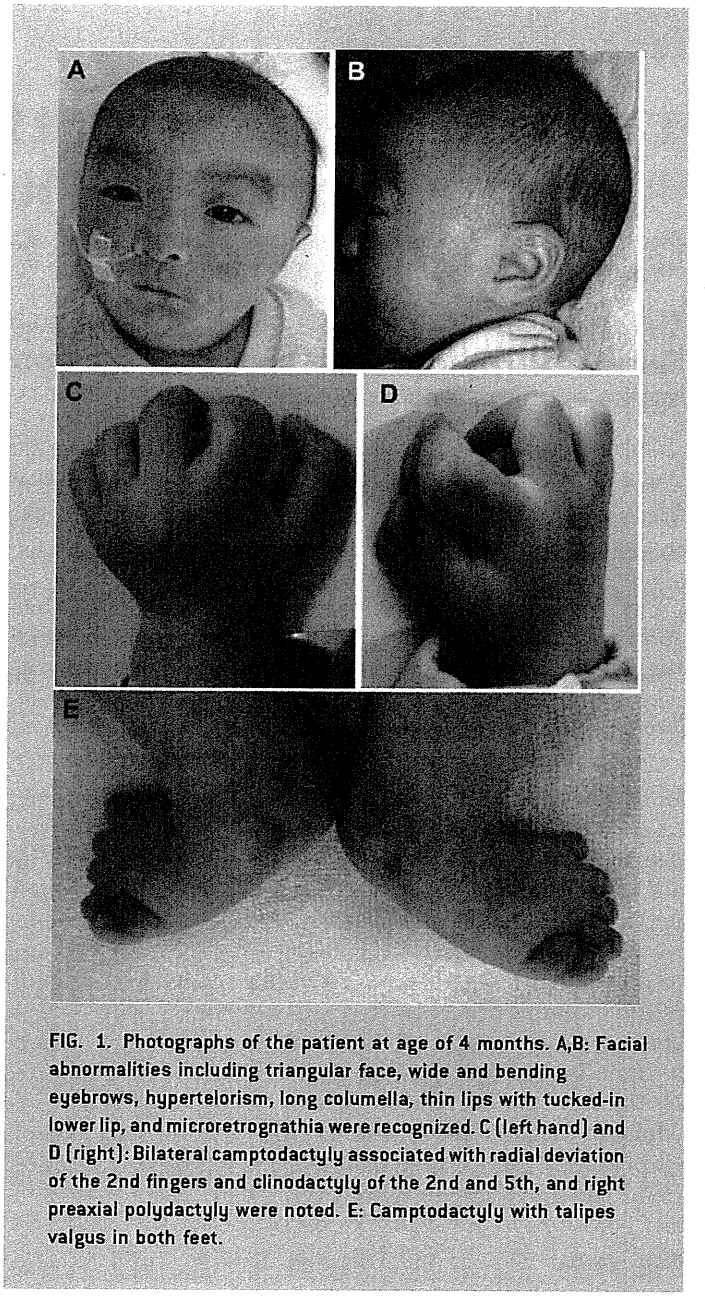

FIG. 1. Photographs of the patient at age of 4 months. A,B: Facial abnormalities including triangular face, wide and bending eyebrows, hypertelorism, long columella, thin lips with tucked-in lower lip, and microretrognathia were recognized. C (left hand) and D (right): Bilateral camptodactyly associated with radial deviation of the 2nd fingers and clinodactyly of the 2nd and 5th, and right preaxial polydactyly were noted. E: Camptodactyly with talipes valgus in both feet.

CYTOGENETIC AND MOLECULAR ANALYSIS

G-banded chromosomal analysis (550 bands level) of the patient's blood lymphocytes indicated normal karyptype (46,XY) (data not shown). Fluorescence in situ hybridization (FISH) analysis using all chromosomal subtelomeric clones did not show any abnormalities. Array CGH analysis using NimbleGen 385K Array (Roche NimbleGen, Inc., Madison, WI) demonstrated a 6.5-Mb heterozygous deletion at 20q11.2–q12 (UCSC genome coordinates 2006 Mar. version, chromosome 20: 31,269,661–37,782,841 bp) (Fig. 2A). The deletion was also confirmed by FISH using BACs (RP11-322B6 and RP11-782C16 at 21q11.21, and RP11-54P22 and RP11-467J15 at 20q12), RP11-787C16 and RP11-54P22 was deleted while RP11-322B6 and RP11-467J15 were not deleted (Fig. 3). The deletion junction was successfully amplified by PCR using primers (Primer A: 5′-TGA TAG AGC CAA CTG GGT CAT GTG C-3′, Primer C: 5′-TCT AGC TTG CTG AAT TCC TGC CTG A-3′) (Fig. 2B) and its product was sequenced. The deleted region was from 31,274,015 to 37,783,826 bp (6,509,811 bp) with 5-bp overlap (ATAGA) (Fig. 2C). The deletion occured de novo as FISH and

TABLE I. Clinical Manifestations of Reported Cases of 20q11–q12 Deletion

	Calliers' case (4 y, female)	Iqbals' case (2 y, male)	Present case (18 m, male)
General			
Growth retardation	+	+	+
Developmental delay	+	+	+
Autistic behavior	+	+	+
Sensory abnormalities/self-injury	+	+	+
Feeding difficulties	+	+	+
Gastroesophageal reflux	+	+	+
Gastrointestinal abnormalities	+ [Pyloric stenosis]	−	+ [Esophageal hiatus hernia]
Feeding intolerance	+ [Diarrhea, vomiting]	−	−
Dysphagia			+
Food refusal	+		+
Muscle tone	Hypertonia	Normal tone except for difficulty in extending the hips	Normal tone
Hearing loss		+	+
Congenital heart defect	−	−	+
Seizure/epilepsy		−	+
Central nervous system			
Cerebral atrophy	+	+	+
Craniofacial			
Triangular face	+	+	+
Hypertelorism	+	+	+
Hypoplastic alae nasi	+	+	+
Sparse hair	+		+
Down-slanting palpebral fissures	+		+
Long columella	+		+
Short, well-defined philtrum	+		+
Thin lips	+		+
Microretrognathia	+		+
Low-set ears	+		+
Extremities			
Arthrogryposis			+
Preaxial polydactyly			+
Clinodactyly of 5th fingers	+		+
Talipes equinovarus		+	
Talopes valgus			+
Ocular			
Retinal dysplasia			+
Microphthalmia		+	−
Duane anomaly		+	n.d.
Strabismus	+		−
Others			
Genital anomlies		+	−

Shadow indicates common features among three cases. y, year(s); m, month(s); +, positive; −, negative; n.d., not determined.

junction PCRs denied the deletion in parental samples (FISH data not shown and Fig. 2B by PCR using primers A, B, and C [primer B: 5′-AGC TGC TCA AAG TGG GGT ATT CTG G-3′]).

DISCUSSION

In this study, we precisely analyzed the 6.5-Mb deletion at 20q11.2–q12 in a boy, presenting with abnormal hands and feet, retinal dysplasia, and intractable feeding difficulty. Proximal interstitial deletions of 20q11–q12 are very rare. Only two cases have been reported and analyzed either by chromosomal CGH and FISH analysis or BAC array CGH with 1-Mb resolution [Callier et al., 2006; Iqbal and Al-Owain, 2007]. Clinical features are presented in Figure 1 and summarized in Table I. Three deletions are overlapping and the shortest region of overlap is from 20q11.22 to q11.23 (Fig. 3). Common clinical features among three cases are

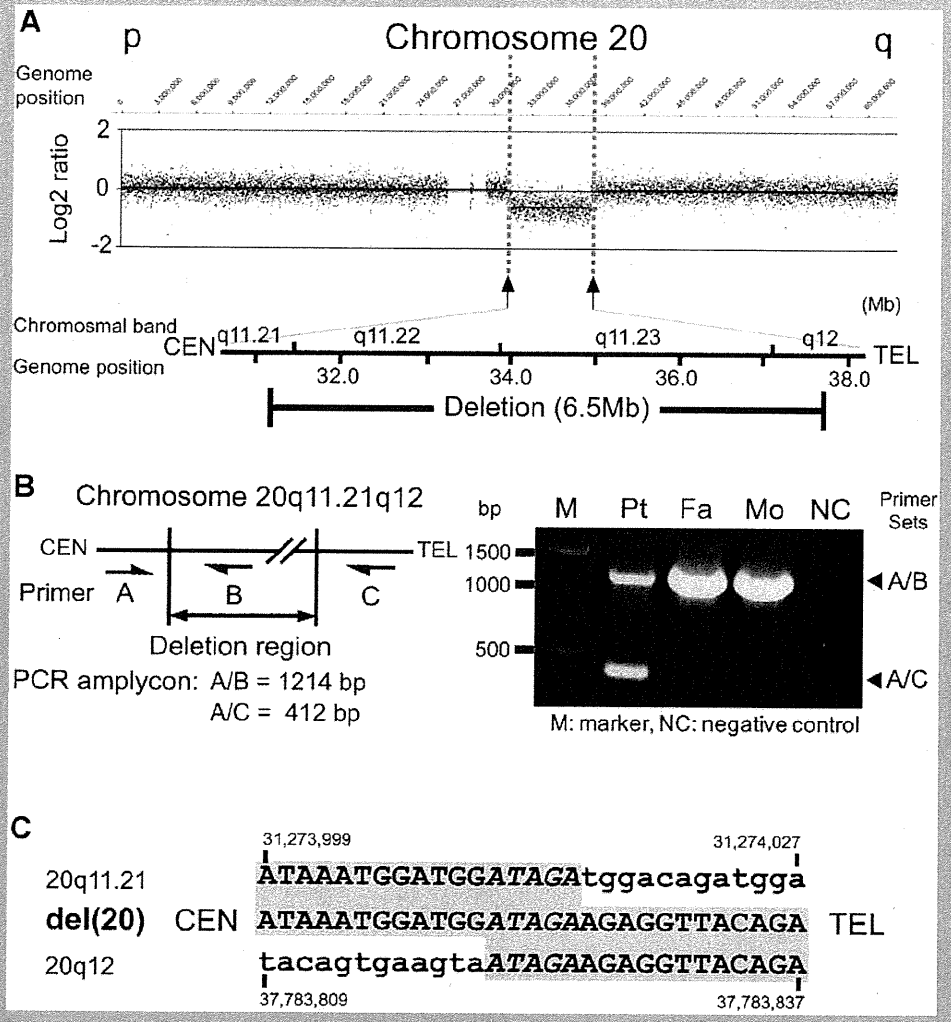

FIG. 2. Analysis of the 20q11.21–q12 deletion. A: High-resolution SNP array revealed the 6.5-Mb deletion at 20q11.21–q12. In the upper part, *Y* and *X* axes indicate probe signal intensity (log 2 ratio) and probe position in chromosome 20, respectively, and in the lower, chromosomal bands together with location of the deletion are shown. B: PCR system (left) to delineate the deletion and its result (right). C: Deletion junction sequence. Upper and lower sequences are normal ones around at proximal [20q11.21] and distal [20q12] deletion breakpoints, respectively. Middle shows the deletion junction in the patient. Gray shadow indicates matched sequences.

growth/developmental retardation, intractable feeding difficulties with GER, cerebral atrophy, and dysmorphic face including triangular face, hypertelorism, and hypoplastic alae nasi. In addition, two out of three patients shared many other facial dysmorphism including sparse hair, downslanting palpebral fissures, long columella, short and well-defined philtrum, thin lips, microretrognathia, and low-set ears. These findings suggest that the 20q11.22–q11.23 deletion can be a recognizable microdeletion syndrome. In addition, unique findings of hands and feet abnormalities as well as retinal dysplasia were found in our patient.

Intractable feeding difficulties in the three patients, is the largest concern for the family, and are speculated to be caused by combined factors: prolonged dysphagia (in our case), aspiration associated with GER (in all three), upper gastrointestinal tract abnormalties (pyloric stenosis [Callier et al., 2006] or esophageal hiatus hernia in our case), vomiting/diarrhea because of feeding intorerance [Callier et al., 2006], sensory abnormalities (in all), and food refusal (in the Callier et al. and our patient).

According to UCSC genome browser (March 2006 assembly), the 6.5-Mb deleted segment identified in our patient encompasses at least 96 known genes, including nine genes related to human disorders. One of these is growth/differentiation factor-5 (*GDF5*, also known as *CDMP1*). This is a protein which belongs to the GDF-subgroup of BMPs and plays an key regulatory role in embryonic skeletal and joint development. *GDF5* abnormalities are known to cause a variety of different skeletal disorders. Interestingly, Everman et al. [2002] and Yang et al. [2008] indicated that functional *GDF5* haploinsufficiency was the culprit of brachydactyly type C (BDC,

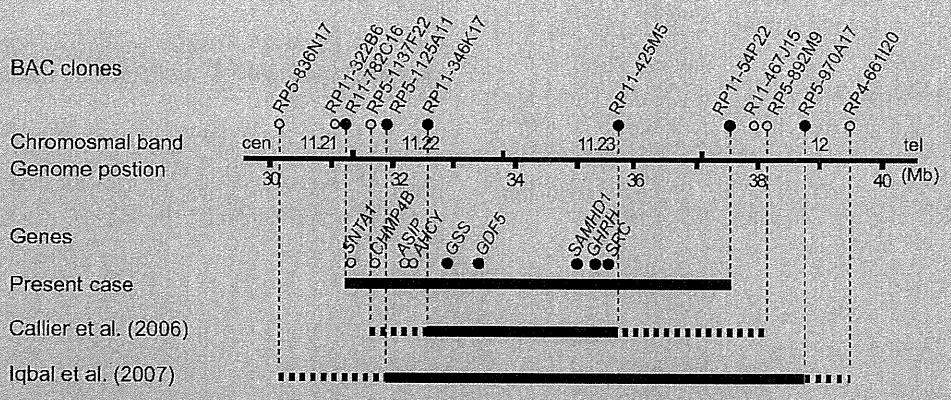

FIG. 3. Shematic presentation of the 20q11–q12 deletions. From top to bottom, BAC clones delineating deletions of all the cases [filled dot: deleted, open dot: not deleted] [Callier et al., 2006; Iqbal and Al-Owain, 2007], chromosomal bands from 20q11.2 to 20q12, genomic position, OMIM genes, and deleted regions of our case and previous ones. Solid and dotted horizontal lines indicate deleted and unconfirmed regions due to the relatively low resolution of the analytical methods.

OMIM #113100) by in vitro studies. As our patient has the *GDF5* haploinsufficiency, he may have the risk for BDC. However, he did not show this manifestation. He did have polydactyly, talipes valgus, and absence of the middle phalanges of the toes, which have been often found in individuals with BDC [Everman et al., 2002; Temtamy and Aglan, 2008]. Our patient did have a fetal akinesia (or hypokinesia) deformation phenotype (FADP). The short neck, hypertelorism, micrognathia, small thorax, postnatal respiratory disturbance, prolonged feeding difficulty, and slender long bone could represent FADP. FADP is a clinically and genetically heterogeneous constellation arising from fetal akinesia or decrease in utero movement due to intrinsic factors including neuropathy, myopathy, and restrictive dermopathy or extrinsic factors that limit fetal movement (e.g., tetragen exposure or fetal crowding) [Witters et al., 2002; Bamshad et al., 2009]. As extrinsic factors (e.g., abnormality of amniotic fluid, fetal crowding, congenital infection, and use of the drug in utero) could not be confirmed in this patient and the arthrogryposis and FADP are accompanied by other organ anomalies and developmental delay, the gene(s) at 20q11.21–q11.23 may be a primary intrinsic cause. Unfortunately, as skeletal malformations in the other two cases having the 20q11.2–q12 deletion were not fully described [Callier et al., 2006; Iqbal and Al-Owain, 2007], it is difficult to discuss the relationship between skeletal features and gene(s) in 20q11.2–q12 deletion.

Retinal dysplasia associated with falciform retinal fold and impaired vision was also noted. Retinal dysplasia is defined as abnormal growth and differentiation of embryonic retina either due to in utero environmental factors such as viral infection, tetragen exposure, retinopathy of prematurity or genetic factors. To our knowledge, this is the first description of retinal dysplasia associated with 20q11.2–q12 deletion.

ACKNOWLEDGMENTS

We are grateful to the patient and his family for their participation and support to this study. Grant-in Aid for Japan Society for the Promotion of Science (JSPS) Fellow (A.N.), Research Grants from the Ministry of Health, Labour and Welfare (N.M.), Grant-in-Aid from the Ministry of Education, Culture, Sports, Science and Technology of Japan (N.M.), and Grant-in-Aid for Scientific Research from JSPS (N.M.).

REFERENCES

Aldred MA, Aftimos S, Hall C, Waters KS, Thakker RV, Trembath RC, Brueton L. 2002. Constitutional deletion of chromosome 20q in two patients affected with albright hereditary osteodystrophy. Am J Med Genet 113:167–172.

Bamshad M, Van Heest AE, Pleasure D. 2009. Arthrogryposis: A review and update. J Bone Joint Surg Am 91:40–46.

Borozdin W, Graham JM Jr, Bohm D, Bamshad MJ, Spranger S, Burke L, Leipoldt M, Kohlhase J. 2007. Multigene deletions on chromosome 20q13.13-q13.2 including SALL4 result in an expanded phenotype of Okihiro syndrome plus developmental delay. Hum Mutat 28:830.

Callier P, Faivre L, Marle N, Thauvin-Robinet C, Sanlaville D, Gosset P, Prieur M, Labenne M, Huet F, Mugneret F. 2006. Major feeding difficulties in the first reported case of interstitial 20q11.22-q12 microdeletion and molecular cytogenetic characterization. Am J Med Genet Part A 140A:1859–1863.

Everman DB, Bartels CF, Yang Y, Yanamandra N, Goodman FR, Mendoza-Londono JR, Savarirayan R, White SM, Graham JM Jr, Gale RP, Svarch E, Newman WG, Kleckers AR, Francomano CA, Govindaiah V, Singh L, Morrison S, Thomas JT, Warman ML. 2002. The mutational spectrum of brachydactyly type C. Am J Med Genet 112:291–296.

Genevieve D, Sanlaville D, Faivre L, Kottler ML, Jambou M, Gosset P, Boustani-Samara D, Pinto G, Ozilou C, Abeguile G, Munnich A, Romana S, Raoul O, Cormier-Daire V, Vekemans M. 2005. Paternal deletion of the GNAS imprinted locus (including Gnasxl) in two girls presenting with severe pre- and post-natal growth retardation and intractable feeding difficulties. Eur J Hum Genet 13:1033–1039.

Iqbal MA, Al-Owain M. 2007. Interstitial del(20)(q11.2q12)—Clinical and molecular cytogenetic characterization. Am J Med Genet Part A 143A:1880–1884.

Kanda T, Murayama K, Kondo I, Kitazumi E, Takahashi K, Nakatani K, Yoneyama A, Yamori Y, Kanda Y. 2005. An estimation chart for the possibility of aspiration in patients with severe motor and intellectual disabilities: Its reliability and accuracy. No To Hattatsu 37:307–316.

Petersen MB, Tranebjaerg L, Tommerup N, Nygaard P, Edwards H. 1987. New assignment of the adenosine deaminase gene locus to chromosome 20q13 X 11 by study of a patient with interstitial deletion 20q. J Med Genet 24:93–96.

Shabtai F, Ben-Sasson E, Arieli S, Grinblat J. 1993. Chromosome 20 long arm deletion in an elderly malformed man. J Med Genet 30:171–173.

Temtamy SA, Aglan MS. 2008. Brachydactyly. Orphanet J Rare Dis 3:15.

Witters I, Moerman P, Fryns JP. 2002. Fetal akinesia deformation sequence: A study of 30 consecutive in utero diagnoses. Am J Med Genet 113:23–28.

Yang W, Cao L, Liu W, Jiang L, Sun M, Zhang D, Wang S, Lo WH, Luo Y, Zhang X. 2008. Novel point mutations in GDF5 associated with two distinct limb malformations in Chinese: Brachydactyly type C and proximal symphalangism. J Hum Genet 53:368–374.

REPORT

Mutations in *POLR3A* and *POLR3B* Encoding RNA Polymerase III Subunits Cause an Autosomal-Recessive Hypomyelinating Leukoencephalopathy

Hirotomo Saitsu,[1,*] Hitoshi Osaka,[2] Masayuki Sasaki,[3] Jun-ichi Takanashi,[4] Keisuke Hamada,[5] Akio Yamashita,[6] Hidehiro Shibayama,[7] Masaaki Shiina,[5] Yukiko Kondo,[1] Kiyomi Nishiyama,[1] Yoshinori Tsurusaki,[1] Noriko Miyake,[1] Hiroshi Doi,[1] Kazuhiro Ogata,[5] Ken Inoue,[8] and Naomichi Matsumoto[1,*]

Congenital hypomyelinating disorders are a heterogeneous group of inherited leukoencephalopathies characterized by abnormal myelin formation. We have recently reported a hypomyelinating syndrome characterized by diffuse cerebral hypomyelination with cerebellar atrophy and hypoplasia of the corpus callosum (HCAHC). We performed whole-exome sequencing of three unrelated individuals with HCAHC and identified compound heterozygous mutations in *POLR3B* in two individuals. The mutations include a nonsense mutation, a splice-site mutation, and two missense mutations at evolutionally conserved amino acids. Using reverse transcription-PCR and sequencing, we demonstrated that the splice-site mutation caused deletion of exon 18 from *POLR3B* mRNA and that the transcript harboring the nonsense mutation underwent nonsense-mediated mRNA decay. We also identified compound heterozygous missense mutations in *POLR3A* in the remaining individual. *POLR3A* and *POLR3B* encode the largest and second largest subunits of RNA Polymerase III (Pol III), RPC1 and RPC2, respectively. RPC1 and RPC2 together form the active center of the polymerase and contribute to the catalytic activity of the polymerase. Pol III is involved in the transcription of small noncoding RNAs, such as 5S ribosomal RNA and all transfer RNAs (tRNA). We hypothesize that perturbation of Pol III target transcription, especially of tRNAs, could be a common pathological mechanism underlying *POLR3A* and *POLR3B* mutations.

Congenital hypomyelinating disorders form a heterogeneous group of central nervous system leukoencephalopathies that is characterized by abnormal myelin formation. Although these conditions are readily recognized by brain magnetic resonance imaging (MRI), many cases are not diagnosed correctly.[1] Several syndromes affecting myelination, such as hypomyelination with hypodontia and hypogonadotropic hypogonadism (4H) syndrome (MIM 612440) and hypomyelination with atrophy of the basal ganglia and cerebellum (H-ABC) (MIM 612438), have been described.[2–5] We have recently reported a hypomyelinating syndrome characterized by diffuse cerebral hypomyelination with cerebellar atrophy and hypoplasia of the corpus callosum (HCAHC).[6] Individuals with HCAHC do not show hypodontia or atrophy of the basal ganglia, which are observed in 4H syndrome and H-ABC; however, diffuse hypomyelination, atrophy, or hypoplasia of the cerebellum and corpus callosum are overlapping features of these three syndromes, suggesting that there might be a common underlying pathological mechanism.

Here, we report on four individuals with HCAHC from three unrelated families (Figure 1A; Table 1). Clinical information and peripheral blood or saliva samples were obtained from the family members after obtaining written informed consent. Experimental protocols were approved by the Institutional Review Board of Yokohama City University. To identify pathogenic mutations, we performed whole-exome sequencing of three probands from three unrelated families (individuals 1, 3, and 4). DNAs were captured with the SureSelect Human All Exon 50Mb Kit (Agilent Technologies, Santa Clara, CA) and sequenced with one lane per sample on an Illumina GAIIx (Illumina, San Diego, CA) with 108 bp paired-end reads. Image analysis and base calling were performed by sequence control software real-time analysis and CASAVA software v1.7 (Illumina). A total of 90,014,368 (individual 1), 86,942,264 (individual 3), and 92,168,758 (individual 4) paired-end reads were obtained and aligned to the human reference genome sequence (GRCh37/hg19) with MAQ[7] and NextGENe software v2.00 with sequence condensation by consolidation (SoftGenetics, State College, PA). This approach resulted in more than 88% of target exomes being covered by ten reads or more (see Table S1, available online). Single nucleotide variants (SNVs) were called with MAQ and NextGENe. Small insertions and deletions were

[1]Department of Human Genetics, Yokohama City University Graduate School of Medicine, 3-9 Fukuura, Kanazawa-ku, Yokohama 236-0004, Japan; [2]Division of Neurology, Clinical Research Institute, Kanagawa Children's Medical Center, 2-138-4 Mutsukawa, Minami-ku, Yokohama 232-8555, Japan; [3]Department of Child Neurology, National Center of Neurology and Psychiatry, 4-1-1 Ogawahigashi-cho Kodaira, Tokyo 187-8551, Japan; [4]Department of Pediatrics, Kameda Medical Center, 929 Higashi-cho, Kamogawa-shi, Chiba 296-8602, Japan; [5]Department of Biochemistry, Yokohama City University Graduate School of Medicine, 3-9 Fukuura, Kanazawa-ku, Yokohama 236-0004, Japan; [6]Department of Molecular Biology, Yokohama City University Graduate School of Medicine, 3-9 Fukuura, Kanazawa-ku, Yokohama 236-0004, Japan; [7]Department of Neurology, Kameda Medical Center, 929 Higashi-cho, Kamogawa-shi, Chiba 296-8602, Japan; [8]Department of Mental Retardation and Birth Defect Research, National Institute of Neuroscience, National Center of Neurology and Psychiatry, 4-1-1 Ogawahigashi-cho Kodaira, Tokyo 187-8551, Japan
*Correspondence: hsaitsu@yokohama-cu.ac.jp (H.S.), naomat@yokohama-cu.ac.jp (N.M.)
DOI 10.1016/j.ajhg.2011.10.003.

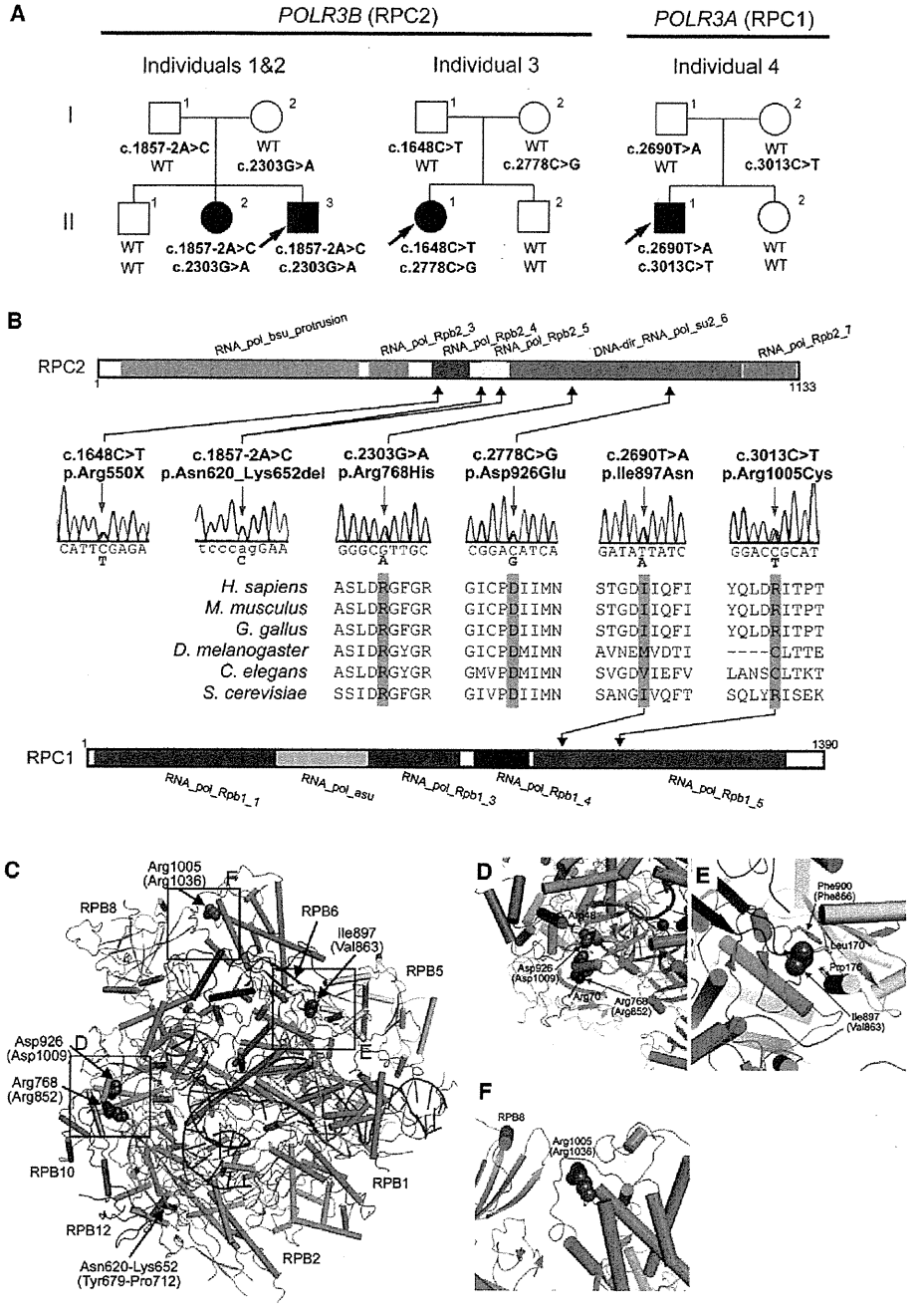

Figure 1. Mutations in *POLR3B* and *POLR3A*

(A) Pedigrees of four kindreds with HCAHC are shown. We identified four mutations in *POLR3B* encoding RPC2 in three individuals from two unrelated families and two mutations in *POLR3A* encoding RPC1 in one family. The segregation of each mutation is shown.

(B) Schematic representation of RPC2 (upper) and RPC1 (lower) proteins with Pfam domains (from Ensembl). Locations of each amino-acid-altering mutation are depicted with electropherograms. All of the missense mutations occurred at evolutionally conserved amino acids. Homologous sequences were aligned with the CLUSTALW website.

(C–F) 3D representations of RPC1 and RPC2 mutations. Mutated amino acids in RPC1 and RPC2 are shown along with their equivalent positions in the homologous RPB1 and RPB2 subunits of RNA Polymerase II (amino acid and its position in parenthesis). The structure and positions of mutations are illustrated by PyMOL with the crystal structure (PDB accession number 3GTP). RPB3, RPB9, and RPB11 subunits, which are specific to RNA Polymerase II, have been omitted from the figure. RPB1 is shown in green, RPB2 in sky blue, RPB5 in yellow, RPB6 in dark blue, RPB8 in pink, RPB10 in orange, RPB12 in purple, DNA in brown, and RNA in red. Amino acids that interact with mutated amino acids are also shown.

Table 1. Clinical Features of the Individuals

Clinical Features	Individual 1	Individual 2	Individual 3	Individual 4
Genes	*POLR3B*	*POLR3B*	*POLR3B*	*POLR3A*
Mutations, DNA	c.1857-2A>C, c.2303G>A	c.1857-2A>C, c.2303G>A	c.1648C>T, c.2778C>G	c.2690T>A, c.3013C>T
Mutations, protein	p.Asn620_Lys652del, p.Arg768His	p.Asn620_Lys652del, p.Arg768His	p.Arg550X, p.Asp926Glu	p.Ile897Asn, p.Arg1005Cys
Gender	M	F	F	M
Current age (years)	27	30	16	17
Intellectual disability	mild	mild	moderate	mild
Cognitive regression	–	–	–	–
Seizures	–	–	–	–
Initial motor development	normal	normal	normal	normal
Age of onset (years)	3	3	2	4
Motor deterioration	–	–	–	+
Wheelchair use	–	–	–	+
Optic atrophy	–	–	–	–
Myopia	+	+	–	+
Nystagmus	+	+	–	–
Abnormal pursuit	+	+	+	–
Vertical gaze limitation	+	+	+	–
Dysphagia	–	–	+	–
Hypersalivation	–	–	–	–
Cerebellar signs	+	+	+	+
Tremor	–	+	+	+
Babinski refex	–	–	–	–
Spasticity	–	–	mild	–
Peripheral nerve involvement	–	–	–	–
Nerve biopsy	NA	NA	NA	NA
Hypodontia	–	–	–	–
Hypogonadism	+	+	–	–

NA is an abbreviation for not available.

detected with NextGENe. Called SNVs were annotated with SeattleSeq Annotation.

We adopted a prioritization scheme to identify the pathogenic mutation in each individual, similar to the approach taken by recent studies (Table S2).[8–10] First, we excluded the variants registered in the dbSNP131 or 1000 Genome Project from all the detected variants. Then, SNVs commonly detected by MAQ and NextGENe analyses were selected as highly confident variants; 364 to 374 SNVs of nonsynonymous (NS) or canonical splice-site (SP) changes, along with 113 to 124 small insertions or deletions (indels), were identified per individual. We also excluded variants found in our 55 in-house exomes, which are derived from 12 healthy individuals and 43 individuals with unrelated diseases, reducing the number of candidate variants to ~250 per individual. Assuming that HCAHC is an autosomal-recessive disorder based on two affected individuals in one pedigree (individuals 1 and 2), we focused on rare heterozygous variants that are not registered in the dbSNP or in our in-house 55 exomes.

We surveyed all genes in each individual for two or more NS, SP, or indel variants. We found three to eight candidate genes per individual (Table S2). Among them, only *POLR3B* encoding RPC2, the second largest subunit of RNA Polymerase III (Pol III), was common in two individuals (individuals 1 and 3). The inheritance of the variants in *POLR3B* (transcript variant 1, NM_018082.5) was examined by Sanger sequencing. In individual 1, we confirmed that a canonical splice-site mutation (c.1857-2A>C [p.Asn620_Lys652del]), 2 bp upstream of exon 18, was

inherited from his father, and that a missense mutation (c.2303G>A [p.Arg768His]) in exon 21 were inherited from his mother (Figure 1A). The two mutations were also present in an affected elder sister (individual 2) but not present in a healthy elder brother. In individual 3, we confirmed that a nonsense mutation (c.1648C>T [p.Arg550X]) in exon 16 was inherited from her father and that a missense mutation (c.2778C>G [p.Asp926Glu]) in exon 24 was inherited from her mother (Figure 1A). The two mutations were not present in a healthy younger brother. To examine the mutational effects of c.1857-2A>C and c.1648C>T, reverse transcription PCR and sequencing with total RNA extracted from lymphoblastoid cells derived from the individuals was performed as previously described.[11] We demonstrated that the c.1857-2A>C mutation caused deletion of exon 18 from the *POLR3B* mRNA (Figures 2A–2C), resulting in an in-frame 33 amino acid deletion (p.Asn620_Lys652del) from RPC2 (Figure 1B). In addition, the mutated transcript harboring the nonsense mutation (c.1648C>T) was found to be expressed at a much lower level compared with the wild-type transcript (Figure 2D). The expression level of the mutated transcript was increased after treatment with 30 μM cycloheximide (CHX),[11] which inhibits nonsense-mediated mRNA decay (NMD), indicating that the mutant transcript underwent NMD (Figure 2D). The two missense mutations (p.Arg768His and p.Asp926Glu) found in the three individuals occurred at evolutionary conserved amino acids (Figure 1B). Among the other candidate genes in individuals 1 and 3, *MSLN* (MIM 601051), encoding mesothelin isoform 1 preproprotein that is cleaved into megakaryocyte potentiating factor and mesothelin, is a potential candidate in the family of individual 1 as its homozygous variant segregated with the phenotype; however, it is expressed in epithelial mesotheliomas, and the mutation affects less conserved amino acid (Table S3). The other candidate genes' variants did not cosegregate with the phenotype. Thus, mutations in *POLR3B* are most likely to cause HCAHC in two families.

In individual 4, in whom no *POLR3B* mutations were found, there were six candidate genes for an autosomal-recessive model. Among them, *POLR3A* (MIM 614258, GenBank accession number NM_007055.3), harboring two missense mutations, appeared to be a primary candidate because it encodes the largest subunit of Pol III (RPC1) (Figure 1A and Table S2). By Sanger sequencing, we confirmed that a missense mutation (c.2690T>A [p.Ile897Asn]) in exon 20 was inherited from his father and that another missense mutation (c.3013C>T [p.Arg1005Cys]) in exon 23 was inherited from his mother (Figure 1A). The two mutations were not present in a healthy younger sister. The two missense mutations (p.Ile897Asn and p.Arg1005Cys) occurred at relatively conserved amino acids (Figure 1B). In total, we found four mutations in *POLR3B* and two mutations in *POLR3A*. Evaluation of the missense mutations by PolyPhen-2 program showed that three mutations (p.Arg768His,

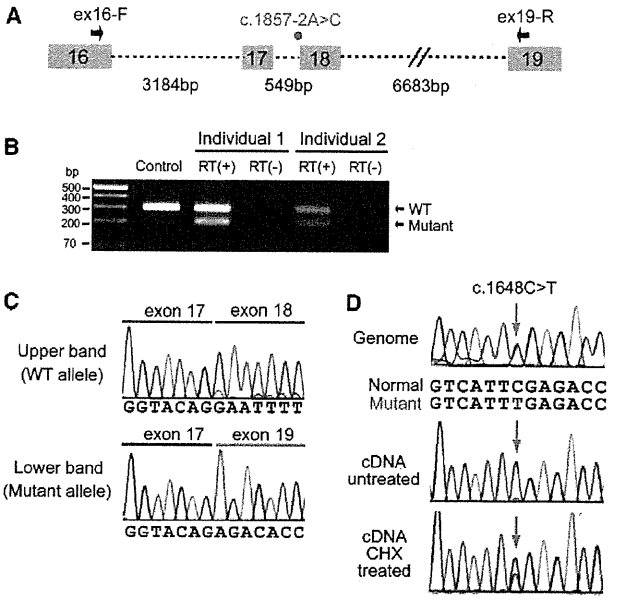

Figure 2. Effects of Splice-Site and Nonsense Mutations in *POLR3B*

(A) Schematic representation of the genomic structure of *POLR3B* from exon 16 to 19. Exons, introns, and primers are shown by boxes, dashed lines, and arrows, respectively. The mutation in intron 17 is depicted as a red dot.

(B) RT-PCR analysis of individuals 1 and 2 with c.1857-2A>C and a normal control. Two PCR products were detected from the individual's cDNA: the upper band is the wild-type (WT) transcript, and the lower band is the mutant. Only a single wild-type amplicon was detected in the control.

(C) Sequence of WT and mutant amplicons clearly showed exon 18 skipping in the mutant allele.

(D) Analysis of the c.1648C>T mutation. Sequence of PCR products amplified with genomic (upper), cDNA from untreated cells (middle), and cDNA from CHX treated cells (lower) as a template. Although untreated cells show extremely low levels of c.1648C>T mutant allele expression, cells treated to inhibit NMD show significantly increased levels of mutant allele expression.

p.Asp926Glu, and p.Ile897Asn) were probably damaging and that p.Arg1005Cys is tolerable. The c.2303G>A mutation (*POLR3B*) was found in one allele out of 540 Japanese control chromosomes. The remaining five mutations were not detected in 540 Japanese control chromosomes, indicating that the mutations are very rare in the Japanese population. Among the other candidate genes in individuals 4, *IGSF10*, a member of immunoglobulin superfamily, is a potential candidate because its variants segregated with the phenotype (Table S3); however, considering a close relationship between *POLR3A* and *POLR3B*, and the fact that *POLR3A* mutations have been recently reported in hypomyelinating leukodystrophy (see below),[12] *POLR3A* abnormality is the most plausible culprit for HCAHC in individual 4.

The structure of Pol III[13,14] and Pol II[15,16] is highly homologous, especially in the largest subunits. Thus, we extrapolated the mutations of RPC1 or RPC2 onto the structure of yeast Pol II (Protein Data Bank [PDB] accession number 3GTP)[17] (Figure 1C). RPB1 and RPB2 subunits of